Techniques for Contact-Based Structural Health Monitoring with Multirotor Unmanned Aerial Vehicles

ROBERT WATSON, TAIYI ZHAO, DAYI ZHANG, MINA KAMEL, CHARLES MACLEOD, GORDON DOBIE, GARY BOLTON, ANTOINE JOLY, S. GARETH PIERCE AND JUAN NIETO

ABSTRACT

Use of Unmanned Aerial Vehicles (UAVs) for Structural Health Monitoring (SHM) has become commonplace across civil and energy generation applications with hazardous or time-consuming inspection processes. Expanding upon surface screening offered by non-contact remote visual inspection UAVs, systems are now beginning to incorporate contact-based Non-Destructive Evaluation (NDE) transducers to detect and monitor incipient sub-surface flaws. However, challenges to environmental interaction using conventional multirotor platform dynamics amid aerodynamic disturbances have frustrated efforts for stable and repeatable sensor placement.

Herein, two distinct UAV systems are evaluated as a means to overcome these challenges. The first utilizes vectored thrust with a tri-copter layout. It may dynamically re-orient dual-axis tilting propellers to directly effect interaction force and deploy dry-coupled ultrasonic thickness measurement across omnidirectional targets. In static point and rolling scan measurement, laboratory tests demonstrate mean absolute error below 0.1 mm and 0.3 mm, respectively. The second UAV uses rigidly affixed multi-directional propellers to reverse and redirect its net thrust. Landing atop cylindrical structures it may crawl around their circumference, supporting itself without magnetic or vacuum adhesion. Arbitrary static position is maintained to within a mean deviation of 0.7 mm. Lastly, comparative discussion of each system informs strategies for further development of contact-based aerial SHM and its adoption to industrial practice.

INTRODUCTION

Robotic and automated systems have become vital tools in structural health monitoring and non-destructive evaluation applications. Their effectiveness in dirty, dull, and dangerous work is well established [1]. As tools for quantitative data capture,

Robert Watson, Taiyi Zhao, Dayi Zhang, Charles MacLeod, Gordon Dobie & S. Gareth Pierce, Centre for Ultrasonic Engineering, University of Strathclyde, 204 George Street, Glasgow, G1 1XW, UK.
Mina Kamel, Voliro AG, Weinbergstrasse 35, 8092 Zurich, Switzerland
Gary Bolton, National Nuclear Lab., Chadwick House, Warrington, WA3 6AE, UK
Antione Joly, EDF Energy R&D UK Centre, 81-85 Station Road, Croydon, CR0 2AJ, UK
Juan Nieto, Mixed Reality & AI Lab, Talstrasse 9, 8001 Zurich, Switzerland

they inform predictive structural health models and permit safe, cost-effective, repair scheduling to correct issues before they become critical. Recently, UAVs have seen widespread adoption in SHM of large-scale civil and energy generation structures. Rapid visual survey by UAV can preclude unnecessary manned work at height, entry to unstable structures, or exposure to radiological and chemical contaminants. Their use is prevalent in operations and management (O&M) of hydroelectric dams [2], wind turbines [3], bridges [4], and nuclear facilities [5]. Extensions using photogrammetric reconstruction track asset geometry changes over time [6] or monitor deformation under loading [7]. However, these outer-surface inspections may only indirectly infer underlying structural status. Reliance on non-contact techniques limits aerial SHM relative to the range of applications supported by contact-based NDE sensors [8].

Contact-based aerial inspection requires interaction stability amid aerodynamic disturbances, accurate and repeatable sensor deployment, and full characterization of any resultant signal degradation. Established unidirectional thrust (UDT) UAVs are under-actuated and must maneuver the entire craft to exert 3D stabilization forces, incurring undesired sensor motion and degrading data capture. Strategies utilizing compliant probe arms [9], supportive frames [10], or magnetic adhesion [11] increase UAV mass, size and risk of aerial snagging, and limit their applicability.

In response, a UAV may utilize Multi-Directional Thrust (MDT) or Vectored Thrust (VT) topologies. Both approaches can yield fully or over-actuated UAVs, capable of independent 3D force and torque generation and incorporating redundancy in this ability, respectively. In MDT craft, multiple propellers in a range of orientations are rigidly affixed to the airframe. By superposition and courter-action of undesired components, their net effect can meet a desired force-torque setpoint. In VT craft, propellers are mounted to the airframe via dynamic actuators and may be re-oriented in flight to meet the force-torque setpoint. Direct setpoint generation typically grants VT superior efficiency versus MDT UAVs but increases control complexity.

Aerial SHM systems thus frequently couple a serial robotic effector with an MDT platform to increase operability, targeting ultrasonic corrosion monitoring in storage tanks and elevated pipework [12], or eddy current based weld seam localization [13]. However, this approach can significantly increase system size and mass. Manipulator motion also introduces reaction disturbances. Parallel manipulators aboard UDT [14] and VT platforms [15] face similar challenges, though early results show significant potential for hyper-redundant aerial tool placement in the latter case.

Low-power perching strategies may improve UDT UAV contact stability. Landing atop a pipe rack then using a lightweight serial manipulator to reach the underside, [16] provides long duration UAV presence but its wheel-roller geometry prevents stable landing on single pipe structures. Delivering ultrasonic NDE to single pipes up to 300 mm diameter, [17] uses a soft robotic gripper inch-worm mechanism to propel a UAV along the top surface. However, reliance on friction prevents activity outside ±30° of vertical and precludes NDE of corrosion in the side-walls or bottom.

In recognition of these challenges to contact-based aerial SHM, this paper discusses two systems, separately employing VT and MDT UAVs. An overview of each system is given, describing its application and operating principles. Experimental assessment of their SHM capability through application focused testing follows. Finally, contextualized discussion of results informs practical recommendations in support of development and adoption of contact-based aerial inspection processes.

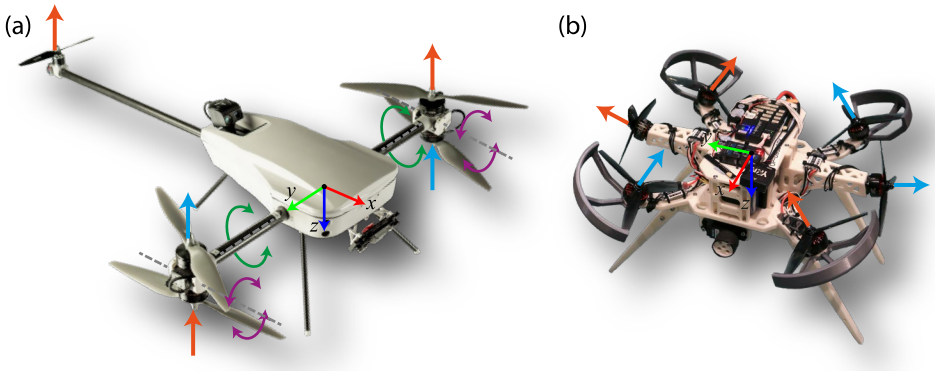

Figure 1. Contact-based SHM platforms (a) Voliro VT UAV platform. (b) MDT UAV-Crawler hybrid. Annotations show nominal propeller thrust direction. Orange rotates clockwise: blue, anti-clockwise.

SYSTEM DESCRIPTION: VOLIRO

The Voliro [18] platform, as in Figure 1(a), is developed as a generic solution for contact-based aerial interaction. Here, as previously reported in [19], it deploys aerial ultrasonic thickness measurement, applicable across targets including petrochemical storage tanks, pipes, steel chimneys, and offshore structures.

Aerial interactions are supported through an over-actuated VT architecture. Its two main rotor pairs provide lift and may be independently rotated about two axes, as shown in Figure 1, for non-horizontal hovering and alignment with omnidirectional surfaces. Opposing spins within each rotor pair, allow generation of a pure thrust force or additional torque component as desired. A reversible tail rotor grants stabilization about the pitch axis. The omnidirectional dynamics of this T-shaped UAV topology allow entry to singe-point contact with surfaces via a lightweight rigid arm extending from its front. Force up to 30 N can be exerted in all directions, rejecting disturbance in up to 12 m/s winds, and supporting the 4 kg craft mass. A custom Px4-based [20] flight controller provides hybrid force-position control under piloted and autonomous flight.

A 5 MHz, dual-element, dry-coupling wheel probe [21], driven by a custom transceiver circuit [9], forms the embedded ultrasonic instrumentation. Exertion of force of 20 N through the probe tire expunges the air-layer between it and the target material, permitting ultrasonic transmission by dry-coupling. This removes the need to carry a couplant gel reservoir. Tire material conformability enables signal transmission at orientations within ±10° of surface normal, superior to ±3° in hard-faced probes [9]. The piezoelectric transmit element is driven by a 180 V single-pulse excitation at a pulse repetition frequency of 100 Hz. Ultrasonic echoes are captured by the receive element, amplified and digitized at 8 bit depth and a sampling frequency of 100 MHz. These are then transferred to an embedded PC running ROS [22] for real-time display on a ground station over Wi-Fi. A post-processing step evaluates material thickness, using the time of flight between backwall echoes and calibrated speed of sound in the target material.

SYSTEM DESCRIPTION: UAV-CRAWLER

The second UAV, as in Figure 1(b), is a novel, specialized platform for NDE transducers such as visual, ultrasonic or pulsed eddy current (PEC) sensors delivered in

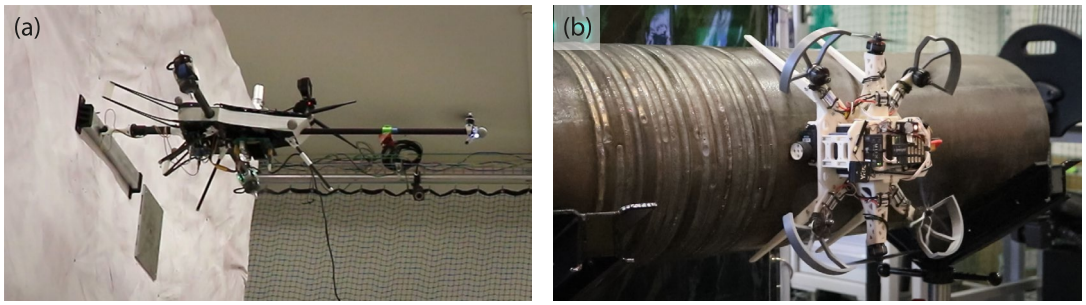

Figure 2. Environment interaction by UAV platforms supporting contact-based inspection.
(a) The Voliro platform scans an ultrasonic wheel probe along a bar sample.
(b) The UAV-crawler holds position on the side of a pipe sample under its own thrust.

contact, or with consistent close-proximity standoff, about the circumference of pipes, storage tanks, pressure vessels or other horizontal cylindrical structures. Target defects include corrosive wall loss, flow accelerated corrosion, and corrosion under insulation.

This prototype uses an MDT configuration, with six 5-inch, fixed-pitch, reversible propellers hexagonally distributed about the airframe. These generate symmetrical thrust in both the forward and reverse spin directions, allowing complete inversion of the output thrust. Four propellers are cambered in by 25° from vertical, while a further two are angled 15° above horizontal. Thus, their net effect may generate up to ±30.8 N vertically and ±28.8 N horizontally relative to the UAV body. This is sufficient to support the 1.84 kg craft, a 300 g payload, and normal contact force above 8 N in all orientations about a target circumference, following landing atop the target then crawling about its surface, without relying on magnetic or vacuum adhesion.

Intimate, multi-point surface contact utilizes two continuous rotation servos for locomotion about the target in a hybrid of MDT UAV and mobile robotic crawler features. These servo wheels form the main interaction points, providing a radial contact force and tangential friction force. The rigid legs provide normal force for roll and yaw axis stabilization and are re-configurable to encompass target diameters above 160 mm. Bounding dimensions of 365 x 340 x 260 mm make this craft far smaller than airborne MDT solutions and significantly reduce required target radial clearance to <180 mm.

The UAV is controlled by a custom version of the PX4 flight stack [20], adapted to the MDT airframe and applying a rigid-body interaction model to define the force-torque setpoint for static equilibrium about the target circumference. The existing Inertial Measurement Unit (IMU) provides the only necessary sensor data for this real-time interaction control, enabling deployment without external positioning systems well suited to industrial environments.

EXPERIMENTAL RESULTS: VOLIRO

Assessment of the Voliro platform considered its ability to perform aerial ultrasonic thickness measurement, targeting two aluminum samples, visible in Figure 2(a), with features representative of large-scale corrosive wall loss. The first of these was a plate sample with outer face dimensions of 292 x 232 mm, a thickness of 8.20 mm, and two 80 mm wide horizontal strips machined from the rear leaving wall thickness of 3.08 mm and 4.47 mm. This is used to assess accuracy of omnidirectional aerial single point

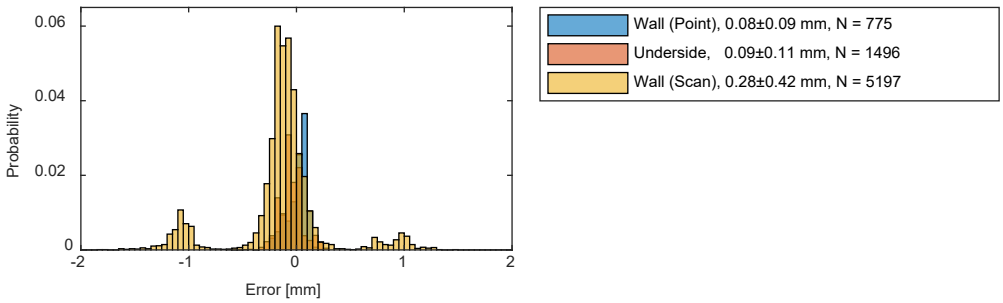

Figure 3. Aerial ultrasonic thickness measurement error distribution across multiple interactions with a vertical wall and the underside of a 45° overhang in static, single-point contact, and a scanning mode across the surface of a vertical wall. Annotations give Mean Absolute Error (MAE) ± std. deviation.

thickness measurements on a vertical wall and on the underside of a 45° overhang. The second sample was a stepped bar with outer face dimensions of 500 x 63 mm. Over 25 equal steps, its thickness ranges from 31.46 mm to 17.60 mm in 1 mm increments, then 17.60 mm to 16.59 mm in 0.1 mm increments. This is used to assess cross-sectional accuracy when scanning along a surface. Reference geometry for both samples is acquired by micron caliper measurement. Projection of the measurement location from the UAV pose estimate along the probe arm to the point of intersection with the sample allows comparison with the ultrasonic readings to evaluate error. Here, UAV pose is generated by fusion of onboard IMU data with position from a Vicon Tracker camera system [23]. Satellite navigation or computer vision solutions may also be used. Further details of this experimental assessment are provided in [19].

Figure 3 profiles ultrasonic measurement error during static single point measurements of the plate sample on a vertical wall and on the underside of a 45° surface. In 3 and 6 instances of static contact, each lasting longer than 2 s and including a range of thicknesses, UAV position was stable to within a mean absolute position deviation of 6.13 mm and 7.49 mm, respectively. Measurement error is similar to that of commercial hand-held ultrasonic thickness gauges [24], [25]. Figure 3 also shows the measurement error of a scan taken in two passes over the bar sample, traversing a total distance of 0.71 m in under 65 s. Here, irregular UAV motion was observed due to sudden changes tire rolling resistance between static and dynamic modes. Uncertainty in the projected measurement location up to a radius of 16.55 mm is also noted to assign readings to adjacent step features, biasing the reference geometry by ±1 mm as in Figure 3. Ultrasonic measurement accuracy is otherwise similar to the static cases and was able to resolve all step features in the swept path. This validates the approach for detection and localization of large-scale, uniform, and mesa-type corrosion features. Smaller features remain ultrasonically detectable but present uncertainty in their localization.

EXPERIMENTAL RESULTS: UAV-CRAWLER

Assessment of the UAV-crawler platform examines its ability to reach and maintain arbitrary static position about a 1.25 m sample of 12.75 inch (324 mm) outer diameter, schedule 80, steel pipe under its own thrust, as in Figure 2(b).

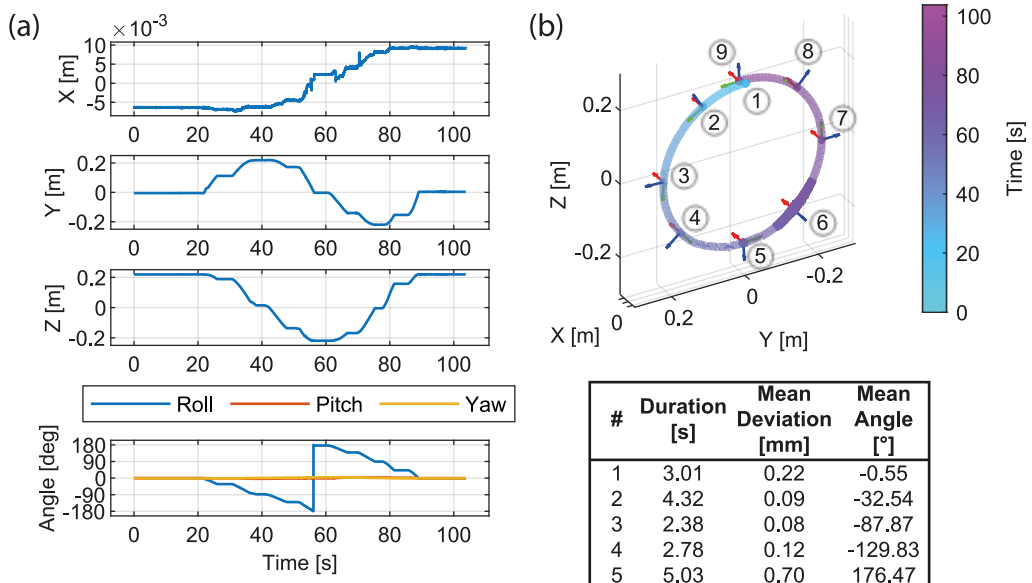

#	Duration [s]	Mean Deviation [mm]	Mean Angle [°]
1	3.01	0.22	-0.55
2	4.32	0.09	-32.54
3	2.38	0.08	-87.87
4	2.78	0.12	-129.83
5	5.03	0.70	176.47
6	2.80	0.11	139.01
7	2.25	0.12	89.62
8	4.07	0.07	42.44
9	3.04	0.23	-2.57

Figure 4. (a) Trajectory of the UAV-crawler platform about the pipe sample. Motion is expressed relative to the pipe center using 'ZYX' Euler angle convention. (b) 3D plot of the inspection path, line color indicates temporal progression. Callouts denote pose variation at static inspection points.

Starting atop the pipe, the craft is piloted around the complete circumference in continuous contact, stopping at 45° increments. Figure 4 plots the position of the UAV during this maneuver, as recorded by a Vicon Tracker camera system [23] and quantifies mean absolute deviation from its average position when commanded to hold stationary. This also gives the clockface angle of the UAV at each of the 9 static points. 0° denotes the top, with positive clock-wise rotation.

As shown, the UAV successfully holds stable position in each location for over 2 s before being piloted onwards, completing the path from leaving the top to returning in under 73 s. Average speed between the static points was 0.024 ms^{-1} and is observed to be smooth and well controlled per Figure 4(a). A 15 mm progression along the pipe x-axis occurs owing to a small speed differential between the two servos responsible for circumferential locomotion. This effect may be deliberately exaggerated to make small corrections to longitudinal pipe position without requiring flight.

Annotation accompanying Figure 4(b) shows mean deviation in static position below 0.25 mm at all points except position 5, where the UAV is directly beneath the sample and partially occluded from view of the Vicon cameras, degrading their measurement. Notably, deviation is lower at points where the UAV is supported by its thrust than at the top of the pipe where the propellers slow and it rests under its own weight to save power. This includes points 3 and 7 where craft weight must be entirely supported by tire friction and lateral thrust, perpendicular to the main vertical thrust used in free-flight and it is most likely to slip. These results therefore serve as strong evidence in validation the UAV-crawler concept for SHM sensor deployment.

DISCUSSION

Experimental results show that both the Voliro platform and the UAV-crawler hybrid successfully maintain stable static contact with representative target structures in a range of orientations. Relative to VT platforms performing single-point contact with a long effector, the multi-point contact strategy allows simplification of both craft design (reducing size and mass) and its control structure. Partial stabilization by contact reaction forces granted the UAV-Crawler mean position deviation under 0.7 mm during static interaction, versus 7.49 mm mean deviation shown by the airborne Voliro. This effect may be leveraged to further reduce undesired motion of an NDE sensor. Moreover, the UAV-crawler approach shows that sensor locomotion through contact-based wheels may also improve controllability versus relying purely on UAV force generation, allowing fine repositioning in NDE of small cracks or pitting. However, reliance on specific horizontal-axis cylindrical geometry limits applicability of the UAV-Crawler. Conversely, the Voliro UAV is a widely deployable solution enabling consistent and cost-effective NDE with minimal knowledge of the target structure.

Future contact-based aerial SHM work may thus focus on low-power transducer delivery and stabilization, leveraging the efficiency and dynamicity of VT craft, with fine-scale corrective motion in contiguous structure contact. More specialized UAV craft emphasizing such features are expected to develop as the technology matures, incorporating additional NDE modes and extending the range of aerial SHM activities.

CONCLUSION

The UAV systems examined in this paper illustrate a range of approaches to airborne SHM and provide quantitative evidence of its practicality. Successful deployment of ultrasonic thickness mapping to omnidirectional structures was conducted using a vectored thrust UAV. A novel platform combining multi-directional reversible thrust propellers with surface crawling ability was also validated for stable NDE deployment around a pipe sample. Final consideration of both UAVs identifies beneficial features for future development, ultimately broadening airborne SHM activity and reducing inspection costs to asset operators across industrial sectors.

ACKNOWLEDGEMENTS

This work was supported by EPSRC funding under the iCASE program, Ref: EP/R512114/1, in collaboration with EDF Energy and the National Nuclear Laboratory.

REFERENCES

[1] D. Lattanzi and G. Miller, ‘Review of Robotic Infrastructure Inspection Systems’, *J. Infrastruct. Syst.*, vol. 23, no. 3, p. 04017004, Sep. 2017, doi: 10.1061/(ASCE)IS.1943-555X.0000353.

[2] G. Buffi, P. Manciola, S. Grassi, M. Barberini, and A. Gambi, ‘Survey of the Ridracoli Dam: UAV–based photogrammetry and traditional topographic techniques in the inspection of vertical structures’, *Geomat. Nat. Hazards Risk*, vol. 8, no. 2, pp. 1562–1579, Dec. 2017, doi: 10.1080/19475705.2017.1362039.

[3] M. Shafiee, Z. Zhou, L. Mei, F. Dinmohammadi, J. Karama, and D. Flynn, 'Unmanned Aerial Drones for Inspection of Offshore Wind Turbines: A Mission-Critical Failure Analysis', *Robotics*, vol. 10, no. 1, Art. no. 1, Mar. 2021, doi: 10.3390/robotics10010026.
[4] A. Khaloo, D. Lattanzi, K. Cunningham, R. Dell'Andrea, and M. Riley, 'Unmanned aerial vehicle inspection of the Placer River Trail Bridge through image-based 3D modelling', *Struct. Infrastruct. Eng.*, vol. 14, no. 1, pp. 124–136, Jan. 2018, doi: 10.1080/15732479.2017.1330891.
[5] L. R. Pinto *et al.*, 'Radiological Scouting, Monitoring and Inspection Using Drones', *Sensors*, vol. 21, no. 9, Art. no. 9, Jan. 2021, doi: 10.3390/s21093143.
[6] S. Zhao, F. Kang, J. Li, and C. Ma, 'Structural health monitoring and inspection of dams based on UAV photogrammetry with image 3D reconstruction', *Autom. Constr.*, vol. 130, p. 103832, Oct. 2021, doi: 10.1016/j.autcon.2021.103832.
[7] D. Erdenebat and D. Waldmann, 'Application of the DAD method for damage localisation on an existing bridge structure using close-range UAV photogrammetry', *Eng. Struct.*, vol. 218, p. 110727, Sep. 2020, doi: 10.1016/j.engstruct.2020.110727.
[8] Ida, Nathan and Meyendorf, Norbert, *Handbook of modern non-destructive testing*. Switzerland: Springer Nature, 2017. [Online]. Available: https://doi.org/10.1007/978-3-319-26553-7
[9] D. Zhang, R. Watson, C. MacLeod, G. Dobie, W. Galbraith, and G. Pierce, 'Implementation and evaluation of an autonomous airborne ultrasound inspection system', *Nondestruct. Test. Eval.*, vol. 0, no. 0, pp. 1–21, Feb. 2021, doi: 10.1080/10589759.2021.1889546.
[10] L. M. González-deSantos, J. Martínez-Sánchez, H. González-Jorge, F. Navarro-Medina, and P. Arias, 'UAV payload with collision mitigation for contact inspection', *Autom. Constr.*, vol. 115, p. 103200, Mar. 2020, doi: 10.1016/j.autcon.2020.103200.
[11] R. A. Mattar and R. Kalai, 'Development of a Wall-Sticking Drone for Non-Destructive Ultrasonic and Corrosion Testing', *Drones*, vol. 2, no. 1, p. 8, Feb. 2018, doi: 10.3390/drones2010008.
[12] M. Á. Trujillo, J. R. Martínez-de Dios, C. Martín, A. Viguria, and A. Ollero, 'Novel Aerial Manipulator for Accurate and Robust Industrial NDT Contact Inspection: A New Tool for the Oil and Gas Inspection Industry', *Sensors*, vol. 19, no. 6, Mar. 2019, doi: 10.3390/s19061305.
[13] M. Tognon *et al.*, 'A Truly-Redundant Aerial Manipulator System With Application to Push-and-Slide Inspection in Industrial Plants', *IEEE Robot. Autom. Lett.*, vol. 4, no. 2, pp. 1846–1851, Apr. 2019, doi: 10.1109/LRA.2019.2895880.
[14] S. Hamaza and M. Kovac, 'Omni-Drone: on the Design of a Novel Aerial Manipulator with Omni-directional Workspace', in *2020 17th International Conference on Ubiquitous Robots (UR)*, Jun. 2020, pp. 153–158. doi: 10.1109/UR49135.2020.9144837.
[15] K. Bodie, M. Tognon, and R. Siegwart, 'Dynamic End Effector Tracking With an Omnidirectional Parallel Aerial Manipulator', *IEEE Robot. Autom. Lett.*, vol. 6, no. 4, pp. 8165–8172, Oct. 2021, doi: 10.1109/LRA.2021.3101864.
[16] A. Suarez, A. Caballero, A. Garofano, P. J. Sanchez-Cuevas, G. Heredia, and A. Ollero, 'Aerial Manipulator With Rolling Base for Inspection of Pipe Arrays', *IEEE Access*, vol. 8, pp. 162516–162532, 2020, doi: 10.1109/ACCESS.2020.3021126.
[17] F. J. Garcia Rubiales, P. Ramon Soria, B. C. Arrue, and A. Ollero, 'Soft-Tentacle Gripper for Pipe Crawling to Inspect Industrial Facilities Using UAVs', *Sensors*, vol. 21, no. 12, Art. no. 12, Jan. 2021, doi: 10.3390/s21124142.
[18] 'Voliro Airborne Robotics'. https://www.voliro.com/ (accessed Jun. 29, 2020).
[19] R. Watson *et al.*, 'Dry Coupled Ultrasonic Non-Destructive Evaluation Using an Over-Actuated Unmanned Aerial Vehicle', *IEEE Trans. Autom. Sci. Eng.*, pp. 1–16, 2021, doi: 10.1109/TASE.2021.3094966.
[20] 'Px4 - Open Source for Drones'. https://px4.io/ (accessed Jun. 29, 2020).
[21] 'Home | Eddyfi'. https://www.eddyfi.com (accessed Oct. 09, 2020).
[22] Open Robotics, 'Robotic Operating System (ROS)'. https://www.ros.org/about-ros/ (accessed Nov. 20, 2020).
[23] Vicon, 'Tracker Motion Capture Software for VR and Object Tracking'. http://www.vicon.com/products/software/tracker (accessed Jun. 30, 2020).
[24] Cygnus instruments, 'Cygnus 2+ Hands-Free'. Accessed: Dec. 02, 2020. [Online]. Available: https://www.cygnusinstruments.co.uk/product/cygnus-2-hands-free-2/
[25] '27MG Ultrasonic Thickness Gage'. https://www.olympus-ims.com/en/27mg/#!cms[tab]=%2F27mg%2Fspecifications (accessed Jun. 29, 2020).